Magnetic structure of $La_2O_3FeMnSe_2$: neutron diffraction and physical property measurements

2013 J. Phys.: Condens. Matter 25 086004

(http://iopscience.iop.org/0953-8984/25/8/086004)

J. Phys.: Condens. Matter **25** (2013) 086004 (6pp) doi:10.1088/0953-8984/25/8/086004

Magnetic structure of $La_2O_3FeMnSe_2$: neutron diffraction and physical property measurements

S Landsgesell[1], E Blumenröther[2] and K Prokeš[1]

[1] Helmholtz Zentrum Berlin, Hahn-Meitner Platz 1, D-14109 Berlin, Germany
[2] I Physikalisches Institut, Georg-August-Universität, Friedrich-Hund-Platz 1, D-37077 Göttingen, Germany

E-mail: landsgesell@helmholtz-berlin.de

Received 3 December 2012, in final form 7 January 2013
Published 31 January 2013
Online at stacks.iop.org/JPhysCM/25/086004

Abstract
We report on the characterization of the mixed layered lanthanum iron manganese oxyselenide $La_2O_3FeMnSe_2$, where Fe and Mn share the same crystallographic position. The susceptibility data show a magnetic transition temperature of 76 K and a strong difference between field cooled and zero field cooled (ZFC) data at low fields. While the ZFC magnetization curve exhibits negative values below about 45 K, hysteresis measurement reveals, after an initial negative magnetic moment, a hysteresis loop typical for ferromagnetic material, pointing to competing ferromagnetic and antiferromagnetic interactions. Resistivity and dielectric permittivity measurements indicate that $La_2O_3FeMnSe_2$ is a semiconductor. We performed x-ray diffraction at 295 K and neutron diffraction at 90 and 1.7 K. The nuclear and magnetic structure was refined in the space group $I4/mmm$ with $a = 4.11031$ (3) Å and $c = 18.7613$ (2) Å at 295 K. We did not detect a structural distortion and the Fe and Mn atoms were randomly distributed. The magnetic order was found to be antiferromagnetic, with a propagation vector $q = (0, 0, 0)$ and magnetic moments of 3.44 (5) μ_B per Fe/Mn atom aligned within the a–b plane. This magnetic order is different with respect to the pure Fe or Mn compositions reported in other studies.

(Some figures may appear in colour only in the online journal)

1. Introduction

In the iron pnictide superconducting (SC) systems, the ground state of the parent phase is metallic and the Fe ion resides in a tetrahedrally coordinated site [1]. On the other hand, the cuprate oxides superconductors show an $S = \frac{1}{2}$ antiferromagnetic (AF) Mott insulator ground state where the transition metal resides in a square planar geometry [2]. Despite these differences there are many features of the pnictides that are shared with the cuprates, such as high T_C values, related compounds that are magnetically ordered and a linear temperature dependence of the resistivity. The difference in the high-temperature type of electrical conduction seems to be correlated with the local environment around Fe atoms, which is different in both groups of the system. While in cuprates the surrounding is planar, in Fe pnictides it is not, promoting metallic-type conduction. The former geometry is found also in the case of the recently widely studied oxychalcogenites with the general formula $Ln_2O_3T_2Ch_2$ (Ln = rare earth, T = Mn, Fe, Co, and Ch = S, Se), [3–15]. Despite the fact that the parent phases of the known Fe superconductors are metals, the physics of these materials reveal more an interplay between itinerant and localized magnetism. It may be that a distant Mott insulator of these materials lurks close by. Indeed, recent work has shown that the oxyselenide compound $La_2O_3Fe_2Se_2$ provides a similar local environment of the Fe ion to that found in the Fe superconductors [3, 4, 9]. However, these materials are AF Mott insulators that undergo a structural transition at $T_N = 90$ K [9]. Of clear interest is here is the doping of this compound in order to investigate whether interesting electronic behavior emerges. However, the doping attempts so far, such as recently synthesized $La_2O_3Fe_{2-x}Mn_xSe_2$ [12], have given no hint of a new superconducting class.

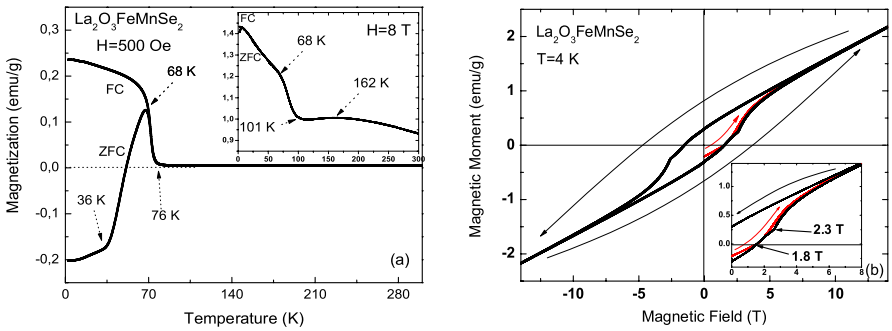

Figure 1. (a) The temperature dependence of the magnetization of $La_2O_3FeMnSe_2$ measured in the range from 2 to 300 K on zero field cooled (ZFC) and field cooled (FC) samples with an external magnetic field of 500 Oe (large panel) and 8 T (inset). (b) Magnetization hysteresis measurement at 4 K from −14 to 14 T. The virgin curve measured on a ZFC sample in the interval from 0 to 14 T is shown in red.

2. Experimental details

We synthesized pure single-phase polycrystalline La_2O_3 $FeMnSe_2$ by using a stoichiometric ratio of dried La_2O_3, Fe, Se and Mn powder, pressing the mixture into a pellet and sealing it in an evacuated quartz ampule. The ampule was heated at 1000 °C for 48 h. The purity of the sample was confirmed by x-ray diffraction on a Bruker D8 (Cu Kα) at room temperature.

We measured the physical properties using a Quantum Design physical property measurement system (PPMS) model 6000. To measure the susceptibility we used the dc vibrating sample magnetometer (VSM) option module; the resistivity and the dielectric permittivity were measured on an Andeen–Hagerling capacity bridge at 1 kHz and 15 V in temperature scans from 2 to 300 K with 2 K min^{-1} using a high-density pellet of the polycrystalline powder.

We collected neutron diffraction data of the La_2O_3FeMn Se_2 sample on the double-axis diffractometer E4 at the Helmholtz-Center in Berlin at 90 and 1.7 K using an incident neutron wavelength of 2.43 Å. The instrument was equipped with a large-area position-sensitive detector that has covered 2θ range of 14°. Twenty-one steps 5° apart were used to cover diffraction angles 10°–110°. Individual frames were re-binned, combined and corrected for background. The data were collected at each of the two temperatures for about 12 h. The frame that contained the two Bragg reflections with the strongest magnetic signal was followed as a function of temperature between 1.7 and 110 K with a shorter exposure time. The crystallographic and magnetic structure details were determined from the best Rietveld-type fits and we performed the Rietveld refinements with the analysis tools of the Fullprof suite [20]. To generate all possible magnetic structures allowed by symmetry of the crystal structure and the experimental propagation vector, we utilized the MODY [21] and BasisReps [20] code.

3. Results and discussion

3.1. Physical properties

In magnetic fields lower than approximately 1.8 T, the magnetization measurements (figure 1(a)) show a clear difference between curves obtained for the zero field cooled (ZFC) and field cooled (FC) samples. The onset of the magnetic order is 76 K for ZFC and FC at 500 Oe. When higher magnetic fields are applied, the onset shifts towards higher temperatures, indicating the presence of ferromagnetic interactions. Also, the nearly flat curve in the paramagnetic regime above 90 K, which exhibits hardly any anomaly at low fields shows a clear hump at higher magnetic fields (approximately at 162 K for 8 T). The biggest difference between high and low magnetic fields is clearly a different temperature dependence below 68 K, where the ZFC of the 500 Oe measurement deviates from the FC curve and below about 45 K becomes negative, resembling a strong diamagnetic-like response. For the ZFC regime one observes about −0.008 μ_B per Fe/Mn site, while for the FC regime the magnetization attains about 0.01 μ_B per Fe/Mn site, both at 2 K. The clear difference in the sign of the magnetization between the ZFC and FC regimes is also visible in the hysteresis measurements (figure 1(b)) at low temperatures, as the starting value for the ZFC curve is negative. Such a negative magnetization has been previously observed on numerous materials including rare-earth [16], actinide [17, 18] and transition-metal [19] systems and has been explained either by the existence of two magnetic sublattices, magnetic domains or a chemical disorder in combination with magnetocrystalline anisotropy that involves magnetic moments leading to competing magnetic interactions. The curve of the magnetic moment of $La_2O_3FeMnSe_2$ at 4 K when an external magnetic field is initially applied (figure 1(b)) shows negative values up to 1.8 T before becoming positive and shows a linear increase at higher fields. The magnetic moment per Fe/Mn site at 14 T increases to 0.09 μ_B. A clear anomaly at 2.3 T is visible on decreasing and increasing magnetic field, which is indicative of a metamagnetic transition. The non-zero remanent magnetization and finite coercive field in the hysteresis measurements point to a ferromagnetic component, while the linear field dependence at higher fields is indicative of AF order. As a result, we encounter the presence of both interactions in our system.

The measurement of the resistivity and the dielectric permittivity from 2 to 300 K without an external magnetic field is shown in figure 2, and these values did not change

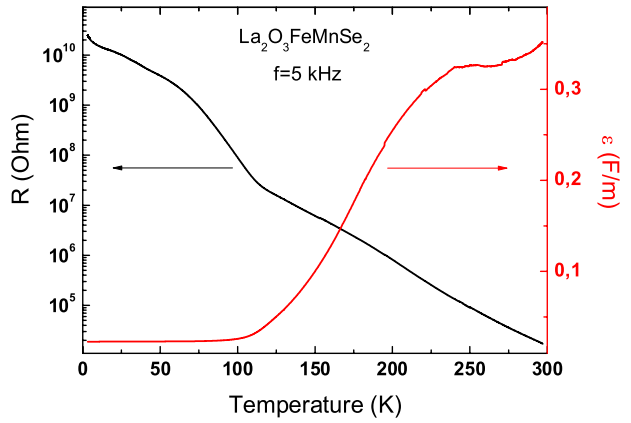

Figure 2. Measurements of the resistivity R (left scale, logarithmic) and the dielectric permittivity ϵ (right scale, linear) of $La_2O_3FeMnSe_2$ from 2 to 300 K without an external magnetic field.

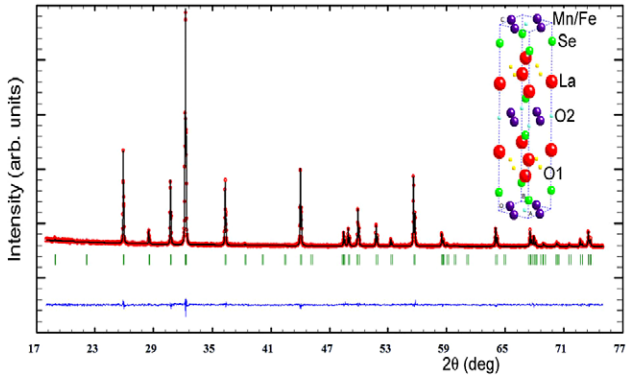

Figure 3. X-ray diffraction of $La_2O_3FeMnSe_2$ at room temperature. Red circles indicate the diffraction values, the black line represents the calculated pattern, the blue line is the difference, the green marks indicate the position of the calculated peaks. The resulting crystal structure is shown in the inset.

in external magnetic fields up to 14 T. As can be seen, the electrical resistivity is of a semiconducting type, showing the thermal activation dependence in the paramagnetic regime. As the temperature is decreased, the resistivity increases by nearly six orders of magnitude between 300 and 2 K. It shows a small hump around 170 K, a clear upturn below 100 K and possibly small upturn at the lowest temperature. In contrast, the electric polarization permittivity, which is non-zero at high temperatures, decreases strongly below 220 K and reaches a negligible value below 100 K.

3.2. Crystal and magnetic structures

Room-temperature x-ray diffraction data shown in figure 3 confirm the high quality of our sample. The best fit to the structural model is isostructural to $La_2O_3Fe_2Se_2$ and gives an excellent agreement with the data. No superstructure was detected, indicating a solid solution with a random distribution of the Fe and Mn atoms in the crystal. The Fe/Mn atoms constitute a so-called checkerboard lattice in this structure, which is shown in the inset of figure 3. There are four atomic sites for the Fe/Mn atoms. We denote these positions as Fe1/Mn1 at ($\frac{1}{2}$ 0 0), Fe2/Mn2 at (0 $\frac{1}{2}$ 0), Fe3/Mn3 at (0 $\frac{1}{2}$ $\frac{1}{2}$) and Fe4/Mn4 at ($\frac{1}{2}$ 0 $\frac{1}{2}$). Each transition metal is surrounded by two in-plane oxygen atoms along one of the a-axes and four Se atoms, which are above and below the planes building the face sharing octahedra. There are three different kinds of in-plane interactions that control the type of magnetic ordering, as displayed in figure 4 and which will be discussed later.

The results of the Rietveld analysis of the x-ray and neutron diffraction data are shown in table 1. The positions of La and Se atoms may vary along the c-axis while the position of the O and Fe/Mn atoms are fixed. Also, the neutron powder diffraction pattern revealed a systematic extinction of reflections when measured at 90 K in the paramagnetic state. This is in agreement with the space group $I4/mmm$. The best fit to the structural model at 90 K using neutron diffraction data is shown in figure 5(a). The refined structural parameters are in good agreement with literature data [9, 15] and are given in table 1. As the temperature is lowered, some of the Bragg reflections increase in intensity. The data shown in figure 6 was collected at the 2-Axis-Diffractometer E4 with a 2D detector. Thirty-one single frames of the 2D detector, centered around $2\theta = 39°$, resulted in an intensity plot that covers (101) and (103) Bragg reflections measured at increasing temperature. The magnetic phase transition is indicated by the appearance of additional intensity in both Bragg reflections at temperatures below T_N.

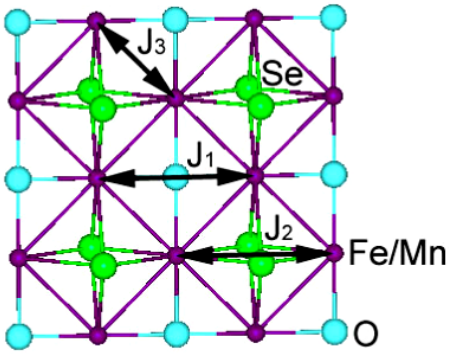

Figure 4. The three main magnetic interactions controlling primarily the magnetic structure within the $La_2O_3Fe_{2-x}Mn_xSe_2$ type of compounds.

The fact that reflections of the magnetic order appear only on the nuclear Bragg positions suggests that the magnetic unit cell has the same size as the nuclear crystallographic unit cell and the corresponding propagation vector is $q = (0, 0, 0)$.[3] In figure 7 we show the temperature dependence of the integrated intensities of the (101) and (103) peaks together with the temperature dependence of the background signal determined from the integration of scattered neutrons in the angle range between the two reflections. The determination

[3] Similar solutions can be found for $q' = (0, 0, 1)$ that result in a different set of symmetry elements but at the end give the same model. The difference between q and q' is that the magnetic moments on the Fe/Mn positions are reversed and that q' would generate reflections on a position that is not allowed in this symmetry ($h + k + l =$ odd) and which we did not measure.

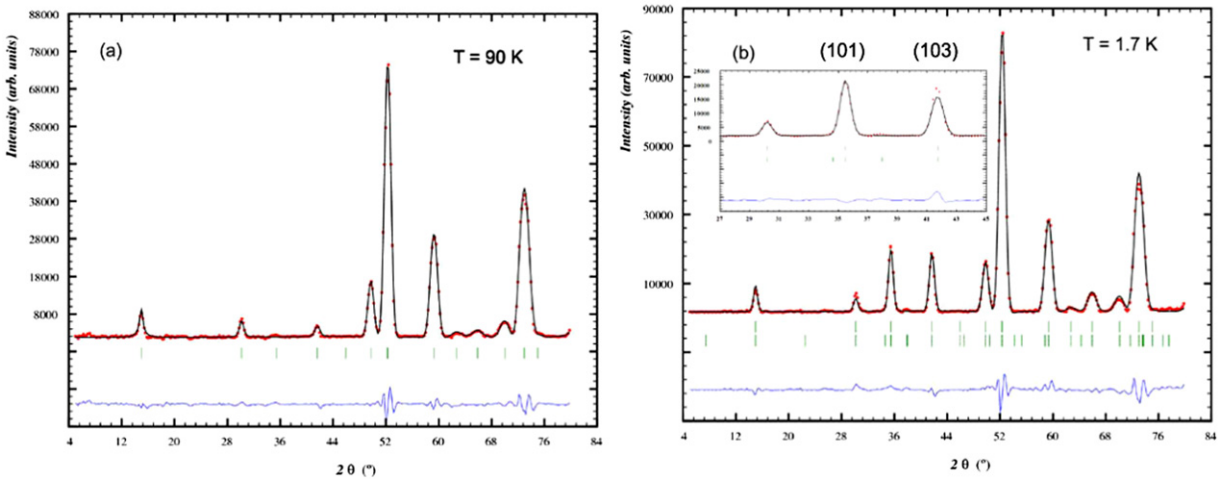

Figure 5. Neutron diffraction data taken at (a) 90 K and (b) 1.7 K. In both panels the red circles indicate the diffraction values, the black line represents the calculated pattern, the blue line is the difference, the green marks indicate the position of the calculated peaks, and for (b) the second line of green marks indicate the peak positions for the magnetic structure model with moments within the basal plane labeled as A_{a-b}. In the inset we show a section of the data fitted with the model where moments point along the c-axis (model A_c).

Table 1. Results from x-ray and neutron Rietveld refinements. The space group we used was $I4/mmm$ (No. 139), the general positions of the atoms are: La ($\frac{1}{2}$ $\frac{1}{2}$ z_{La}), Fe/Mn ($\frac{1}{2}$ 0 0), O(1) ($\frac{1}{2}$ 0 $\frac{1}{4}$), O(2) ($\frac{1}{2}$ $\frac{1}{2}$ 0), Se (0 0 z_{Se}). A_c and A_{a-b} refers to the respective magnetic model with magnetic moments oriented along the c-axis and perpendicular to it, respectively. To demonstrate the quality of our fits we show the crystallographic RF-factor R_f, the contribution of the Bragg factor R_B and the contribution of the magnetic components R_M.

	X-ray (300 K)	Neutrons (90 K)	Neutrons A_c (2 K)	Neutrons A_{a-b} (2 K)
a (Å)	4.11 031 (3)	4.0895 (9)	4.0854 (9)	4.0856 (9)
c (Å)	18.7613 (2)	18.696 (8)	18.684 (6)	18.685 (6)
V (Å^3)	316.966 (5)	312.67 (17)	311.85 (14)	311.89 (14)
La z (c)	0.1857 (2)	0.1840 (3)	0.1818 (3)	0.1831 (3)
Se z (c)	0.0991 (3)	0.0992 (4)	0.0946 (3)	0.0995 (5)
Distance (Fe/Mn–Fe/Mn) (Å)	2.906 (3)	2.892 (3)	2.889 (3)	2.889 (3)
Distance (Fe/Mn–O) (Å)	2.055 (3)	2.045 (3)	2.043 (3)	2.043 (3)
Distance (Fe/Mn–Se) (Å)	2.771 (3)	2.761 (3)	2.701 (3)	2.762 (3)
Distance (La–O(2)) (Å)	3.484 (4)	3.440 (3)	3.397 (3)	3.422 (3)
Distance (La–Se) (Å)	3.330 (3)	3.298 (3)	3.317 (3)	3.285 (3)
Angle (Fe/Mn–Se–Fe/Mn(1)) (deg)	63.25 (3)	63.17 (4)	64.61 (4)	63.07 (4)
Angle (Fe/Mn–Se–Fe/Mn(2)) (deg)	95.73 (3)	95.58 (4)	98.20 (4)	95.41 (4)
$m_{Fe/Mn}$ (μ_B)	—	—	2.59 (2)	3.44 (5)
R_f (%)	4.97	7.9	7.8	7.7
R_B	3.62	5.7	7.8	7.1
R_M	—	—	8.2	6.6

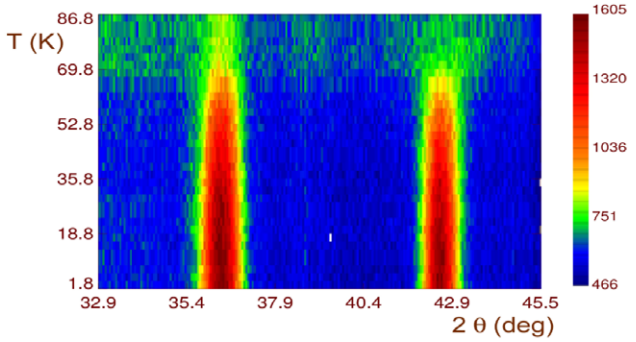

Figure 6. Color-coded temperature dependence of a portion of the diffraction pattern that includes the (101) and (103) Bragg reflections of $La_2O_3FeMnSe_2$ measured with increasing temperature.

of the transition temperature from Bragg reflection intensities is difficult due to the rather long tail of magnetic intensity seen above T_N. This is most probably connected with the 2D character of the magnetism in this material [3–7]. The extrapolation of the temperature dependence above and below the magnetic phase transition leads to $T_N = 72$ (2) K, which is slightly lower than temperature inferred from magnetic bulk measurements. An independent way to determine T_N is possible from the temperature dependence of the background between the two reflections and leads to the identical value. No further magnetic phase transition is evidenced by our data.

All possible magnetic structure models that describe the possible mutual orientation of Fe/Mn magnetic moments within the magnetic unit cell that are in agreement with the paramagnetic space group were generated using the symmetry analysis. There are ten irreducible representations,

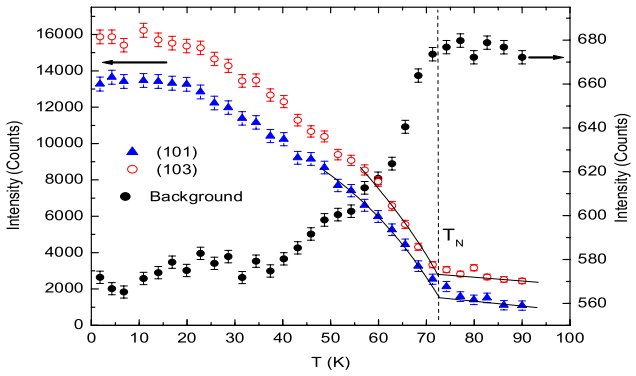

Figure 7. The temperature dependence of the integrated intensities of the (101) and (103) Bragg reflections of $La_2O_3FeMnSe_2$ measured with increasing temperature together with the background between the two reflections. The proposed magnetic phase transition is shown by the dashed line. Full lines through data are a guide to the eye.

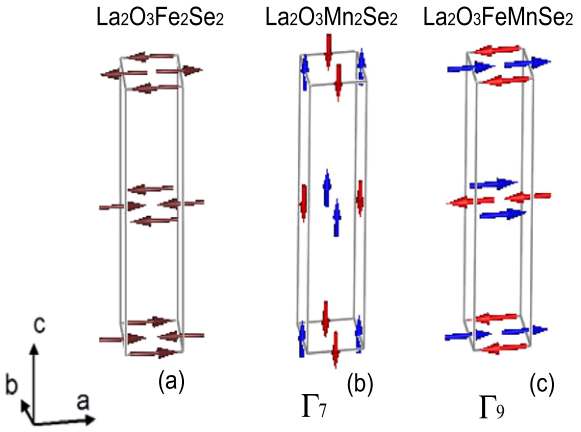

Figure 8. Observed magnetic structure of $La_2O_3FeMnSe_2$ (a) in comparison with possible magnetic structures for $La_2O_3Fe_2Se_2$ with moments along the *c*-axis (b) or perpendicular to the tetragonal direction (c). The AF structure slightly preferred by our study is shown in panel (c). The magnetic structure reported for $La_2O_3Mn_2Se_2$ is displayed in panel (b).

eight are one-dimensional and two are two-dimensional. All other representations fail to allow for magnetic ordering. Those possible magnetic moment configurations fix the spin directions either along or perpendicular to the *c*-axis. Moments can be coupled either ferromagnetically along the *c*-axis (we denote this model as F_c) or antiferromagnetically along the *c*-axis (model A_c). For solutions within the basal plane either ferromagnetic or AF couplings are also possible. We label these models as F_{a-b} and A_{a-b}.

A good agreement with the data can be found for two solutions: A_c and A_{a-b}. These configurations are shown in figures 8(b) and (c), respectively. Both are distinctly different with respect to the magnetic structure found in $La_2O_3Fe_2Se_2$ [9], which is shown in panel figure 8(a). It should be noted that $La_2O_3Mn_2Se_2$ has been found to order also with another magnetic structure, namely with spins oriented along the tetragonal axis and coupled according to panel 8(b) [15]. Both models are based on the same type of coupling between the magnetic moments but differ in the magnetic moment direction and magnitude, with model A_{a-b} giving about 30% larger moments. Numerical parameters of the best fits of these two models as well as the structural parameters are given in table 1. It is well known that in high-symmetry crystal structures the direction of magnetic moments can only be determined with respect to the unique axis [22], in our case with respect to the *c*-axis. The agreement between the data and the best fits in figure 5 is in favor of the in-plane configuration. This is based on the quality factors, on the small fraction of missing intensity due to the AF order on top of the (103) reflection (see inset of figure 5(b)) for the A_c model and on different La and Se positions and other derived structural parameters (e.g. bond angles) as listed in table 1. More consistent results are, in contrast, found for the A_{a-b} model. We therefore conclude that the best agreement is found for a model in which the Fe/Mn moments are confined to the basal plane, as is shown in the figure 5(b).

4. Discussion and conclusions

We have established that the $La_2O_3FeMnSe_2$ system we prepared is single phase and crystallizes in the tetragonal $I4/mmm$ space group. It orders antiferromagnetically below $T_N = 76$ (2) K. It is semiconducting over the whole temperature range studied, with a very low dielectric permittivity at low temperatures. In this work we were able to show that the magnetic properties of $La_2O_3FeMnSe_2$ are strongly dependent on the history of the external fields. For the sample cooled in zero field we observe a negative magnetization measured in 500 Oe up to about 50 K. This phenomenon has been observed previously, and models explaining such an observation are mostly based on the existence of competing interactions due to either chemical disorder or the existence of two magnetic sublattices combined with crystalline anisotropy. As Fe and Mn atoms are randomly distributed, small local deviations from the average distribution might cause the observed peculiar magnetic properties. A delicate energy hierarchy determines the type of the magnetic ordering and the coupling between the magnetic moments in this class of compounds, where the transition metal resides in the double checkerboard lattice with various in-plane exchange paths. Local disturbances may cause changes in the magnetic exchange and magnetic structure on a short scale and may stabilize other types of order. The fact that the negative magnetization reaches only -0.008 μ_B per Fe/Mn site suggests that only about 0.1% of moments contribute to this phenomenon. This is supported by the existence of a small anomaly above T_N in higher fields, reminiscent of the magnetic phase transition in the $La_2O_3FeMnSe_2$ system, which is, however, also AF. It suggests that there may be a certain degree of inhomogeneity present in our sample. Unfortunately, the magnitude of this effect is too small to be studied by techniques available to us. Locally sensitive element probes would be able to resolve this problem. Comparing panels (a) and (b) of figure 8, the AF structure of $La_2O_3FeMnSe_2$ is different from the magnetic structure determined for $La_2O_3Fe_2Se_2$ [9], although in both

compounds an in-plane magnetic moment order is observed. It is also different with respect to the magnetic structure in $La_2O_3Mn_2Se_2$—although the coupling is the same, the moments point in a different direction.

Three main magnetic interactions are shown in figure 4 and must be considered among the Fe^{2+}/Mn^{2+} ions. The first one is the superexchange interaction via the O(2) atoms that are situated in plane and make a 180° Fe/Mn–O–Fe/Mn bond. There are two bonds of this kind for each Fe/Mn. This interaction is labeled as J_1 in figure 4 and is expected to be of an AF nature, similar to the situation in the $La_2O_3Mn_2Se_2$ counterpart, where Goodenough–Kanamori rules [23] apply. The second path is via the double Fe/Mn–Se–Fe/Mn bond, making an angle of about 95° which we denote as J_2. This interaction is expected to be ferromagnetic. The last interaction is the direct interaction labeled as J_3, linking each Fe/Mn site with four other Fe/Mn sites. From the magnetic structure determined in this work it follows that while the J_2 interaction is clearly of a ferromagnetic type, the J_1 is not AF as predicted. It is in both cases ferromagnetic. The remaining J_3 interaction couples Fe/Mn magnetic moments antiferromagnetically. Possible magnetic structures for $La_2O_3T_2Se_2$, T = transition metal compounds have been studied theoretically [4, 7] and it has been shown that the actual structure depends on the strength of the three interactions. Various modifications are possible (see figure 10 in [7], figure 10 in [11] and figure 5 in [4]), according to the type and strength of the leading interaction. We conclude that the strongest interaction in $La_2O_3FeMnSe_2$ appears to be the AF J_3 interaction, leading to an AF structure as shown in figure 8(c). This magnetic structure is identical to the predicted AF structure for the case when $2|J_3| > |J_1|$. The J_2 interaction is, according to calculations, the weakest among the three and is in our case of ferromagnetic nature.

Some concerns exist with respect to the magnetic moment direction. We suggest that rather subtle differences in the recorded diffraction intensities slightly prefer the in-plane configuration rather then the *c*-axis orientation that has been reported to be realized in the $La_2O_3Mn_2Se_2$ counterpart. This conclusion is supported by consistent development of other structural parameters (especially of the bonding angles) upon entering the AF state. The definite proof for such a finding could be obtained only from a single-crystal experiment that should, in contrast to the powder experiment, also be able to determine the in-plane magnetic moment configuration. It should also be noted that a weak ferromagnetic component orthogonal to the AF plane may arise from a Dzyaloshinskii–Moriya interaction and is expected in this symmetry with these superexchange conditions. Another remaining question to be answered is whether Mn and Fe ions carry different magnetic moments. From electron configurations one would expect that Mn^{2+} ions with $3d^5$ should carry larger moments than Fe^{2+} with $3d^6$, both in a high-spin state. Although attempts have been made to resolve this question, the answer remains open as the Fe and Mn atoms are statistically distributed over a single crystallographic position and the method used cannot distinguish between the Fe and Mn spin magnitudes. To resolve this problem, one would need to use another microscopic tool such as muon spin rotation spectroscopy. This may also help in understanding the origin of the negative magnetization curve at ZFC.

Acknowledgments

KP and SL acknowledge the Deutsche Forschungsgemeinschaft for support under the priority program SPP 1458 and contract AR 613/1-2. EB acknowledges the support of HZB during his summer student program stay.

References

[1] Kamihara Y *et al* 2008 *J. Am. Chem. Soc.* **130** 3296
[2] Vaknin D *et al* 1987 *Phys. Rev. Lett.* **58** 2802
[3] Manousakis E *et al* 2010 *Solid State Commun.* **150** 62
[4] Zhu J-X, Yu R, Wang H, Zhao L L, Jones M D, Dai J, Abrahams E, Morosan E, Fang M and Si Q 2010 *Phys. Rev. Lett.* **104** 216405
[5] Clarke S J, Adamson P, Herkelrath S J C, Rutt O J, Parker D R, Pitcher M J and Smura C F 2008 *Inorg. Chem.* **47** 8473
[6] Mayer J M, Schneemeyer L F, Siegrist T, Waszczak J V and Van Dover B 1992 *Angew. Chem.* **31** 1645
[7] Kabbour H, Janod E, Corraze B, Danot M, Lee C, Whangbo M H and Cario L 2008 *J. Am. Chem. Soc.* **130** 8261
[8] Wang C, Tan M Q, Feng C M, Ma Z F, Jiang S, Xu Z A, Cao G H, Matsubayashi K and Uwatoko Y 2010 *J. Am. Chem. Soc.* **132** 7069
[9] Free D G and Evans J S O 2010 *Phys. Rev.* B **81** 214433
[10] Liu R H *et al* 2011 *Phys. Rev.* B **83** 174450
[11] Free D G, Withers N D, Hickey P J and Evans J S O 2011 *Chem. Mater.* **23** 1625
[12] Lei H, Bozin E S, Llobet A, Ivanovski V, Koteski V, Belosevic-Cavor J, Cekic B and Petrovic C 2012 *Phys. Rev.* B **86** 125122
[13] Fuwa Y, Endo T, Wakeshima M, Hinatsu Y and Ohoyama K 2010 *J. Am. Chem. Soc.* **132** 18020
[14] McCabe E E, Free D G, Mendis B G, Higgins J S and Evans J S O 2010 *Chem. Mater.* **22** 6171
[15] Ni N, Climent-Pascual E, Jia S, Huang Q and Cava R J 2010 *Phys. Rev.* B **82** 214419
[16] Murthy P S R, Priolkar K R, Bhobe P A, Das A, Sarode P R and Nigam A K 2010 *J. Magn. Magn. Mater.* **322** 3704
[17] Suski W 2007 *Mater. Sci.—Poland* **25** 333
[18] Gofryk K and Kaczorowski D 2006 *J. Phys.: Condens. Matter* **18** 3887
[19] Hase M, Pomjakushin V Yu, Sikolenko V, Keller L, Luetkens H, Donni A and Kitazawa H 2011 *Phys. Rev.* B **84** 104402
[20] Roisnel T and Rodríguez-Carvajal J 2001 *Mater. Sci. Forum* **378** 118
[21] Sikora W, Bialas F, Pytlik L and Malinowski J 2004 *J. Appl. Crystallogr.* **37** 1015
[22] Rossat-Mignod J 1987 *Neutron Physics* vol 23C, ed K Skold and D L Price (New York: Academic) p 69
[23] Goodenough J B 1955 *Phys. Rev.* **100** 564